Statistical List-mode Reconstruction in Quantitative Dynamic Imaging using the High Resolution Research Tomograph

Arman Rahmim, Stephan Blinder, Ju-Chieh Cheng, and Vesna Sossi

***Abstract*— We have implemented a hybrid ordinary-convergent subsetized (HOCS) list-mode EM reconstruction algorithm suitable for quantitative dynamic (4D) PET imaging. In particular, we have validated the applicability of the proposed list-mode technique to the reconstruction task for the high resolution research tomograph (HRRT). The HOCS list-mode approach is shown to be quantitatively accurate for reconstruction of dynamic frames in the list-mode acquired data. We have also shown that histogram-mode reconstruction using the delayed-events subtraction technique clearly exhibits an over-estimation bias if a sinogram non-negativity constraint is imposed.**

I. INTRODUCTION

In positron emission tomography (PET) systems, there is a continuous effort to increase sensitivity and to improve spatial resolution. This, in turn, brings about the need for different approaches to data collection and image reconstruction in order to make use of the high sampling capabilities of such systems.

Conventional image reconstruction techniques histogram the collected data into sinogram bins. This can be achieved by (i) direct histogram-mode data acquisition, or (ii) by histogramming the events which have been initially collected in list-mode format. The latter has an important advantage in that specification of the timing frames in not required prior to data collection. Still, several other benefits can be gained by reconstructing the list-mode data file directly:

i) *Faster reconstruction:* In studies in which a low number of counts per frame are acquired, the number of events may be in-fact (much) less than the number of lines of response (LORs) in a full sinogram set, especially with high resolution scanners having a very large number of LORs (e.g. 4.5B in the HRRT). Use of list-mode reconstruction techniques implicitly ignores LORs along which counts were not recorded [1], and can therefore considerably improve the reconstruction speed especially for low-statistics frames.

ii) *Preservation of maximum sampling frequency:* When histogram-mode reconstruction methods are used, the data are often *mashed*; i.e. certain 'nearby' LORs are histogrammed into the same sinogram bin in order to reduce the size of the sinogram data. For instance, in the case of the HRRT, with no data compression, the sinogram size is 1.5G bytes. Application of data mashing, however, has been shown to adversely affect image resolution [2]. In the case of list-mode reconstruction, since events are considered one-by-one, sinogram data compression is in principle not needed, thus resulting in preservation of maximum sampling frequency at no extra cost in terms of time and data size.

iii) *Time-of-flight PET:* With the continuous improvements in the technology of PET imaging, time-of-flight (TOF) PET is now being actively reconsidered [3]. TOF PET, especially in whole body scanning, is expected to considerably improve image noise behavior [4]. With the added attribute of time-of-flight measured for the acquired events, increasingly more sinogram bins will be required to take into account the measured TOF information along each LOR. On the contrary, with list-mode reconstruction, one does not require the use of sinogram bins and instead processes the events one-by-one, conveniently including the TOF information.

iv) *Accuracy and convenience in motion correction:* We point out another potential advantage of the list-mode technique: in histogram-mode reconstruction, a motion-corrected LOR will not typically correspond exactly to the center of a sinogram bin, and therefore an interpolation needs to be performed (Fig. 1a). In list-mode reconstruction, however, motion-corrected list-mode event coordinates can be maintained as continuous variables, as we have explained in [5], thus potentially preserving a higher degree of accuracy in the reconstruction task. Furthermore, in histogram-mode reconstruction, the regularly employed sinogram-space has to be extended in order to allow histogramming of *all* motion-compensated LORs including those that do not correspond to existing detector pairs (Fig. 1b), a problem not encountered in list-mode reconstruction [5].

II. CONVERGENT LIST-MODE RECONSTRUCTION

Since the introduction of the ordered subset expectation maximization (OSEM) algorithm for histogram-mode emission tomography [6] there has been considerable interest in accelerated reconstruction techniques. The use of subsets is similarly applicable to list-mode image reconstruction [1]: in this case, the subsets are event-based (instead of LOR-based) and are obtained by sub-dividing the list-mode data into segments that span a fraction of the total duration. We shall use S_l to

Arman Rahmim, Ju-Chieh Cheng, and Vesna Sossi are with Department of Physics and Astronomy, University of British Columbia, Vancouver, BC Canada (e-mail rahmim@physics.ubc.ca, jcheng@physics.ubc.ca, vesna@physics.ubc.ca).

Stephan Blinder is with UBC/Triumf, Vancouver, BC Canada (e-mail blinder@physics.ubc.ca)

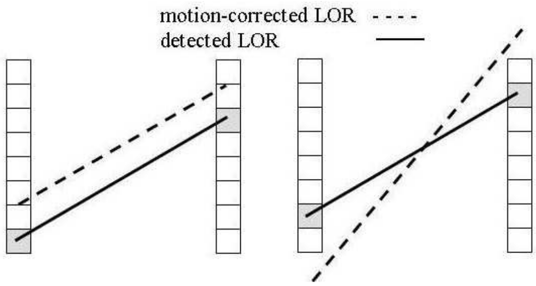

Fig. 1. In histogram-mode reconstruction: (a) a motion-corrected LOR needs to be interpolated into sinogram bins. (b) The sinogram-space also needs to be extended in order to allow histogramming of motion-corrected LORs that do now correspond to actual detector pairs.

Fig. 2. As the current image estimate approaches the maximum likelihood estimators, the image updates become more subset-dependent.

denote the lth list-mode subset (l=1...L), and $\lambda_j^{m,l}$ as the image estimate at voxel j (l=1...J) at the mth iteration and lth subset. The subsetized list-mode expectation maximization (S-LMEM) algorithm is then given by:

$$\lambda_j^{m,l} = \frac{\lambda_j^{m,l-1}}{\sum_{i=1}^{I} p_{ij}} \sum_{k \in S_l} p_{i_k j} \frac{1}{\sum_{b=1}^{J} p_{i_k b} \lambda_b^{m,l-1}} \tag{1}$$

where i_k refers to the LOR along which the kth event is detected, and p_{ij} is the probability of an emission from voxel j being detected along LOR i.

In practice, while the S-LMEM algorithm is seen to initially perform considerably faster than the non-subsetized algorithm, it is typically seen not to converge to a fixed point and instead results in limit cycles [7]. We can explain this using the following observation: each data subset S_l is a different instance of the Poisson process and thus has a distinct maximum-likelihood estimator (MLE) $\widehat{\lambda}_{S_l}$. Depicting a *J*-dimensional space for the image vectors (Fig. 2): at the beginning of the iterative process (where the current estimate λ is far from convergence), each pass through a given subset improves the image estimate nearly independent of the subset, thus explaining the initial effectiveness of the technique. As λ approaches the MLEs, however, the updates take more distinct directions, depending on the subsets, and result in oscillating limit-cycles.

One can argue that convergence properties can be very relevant to clinical medical imaging since algorithm divergence could have unfortunate consequences. For instance, the theoretical analysis of Qi and Huesman [8] in lesion detectability applies *only* to convergent algorithms, whereas no such justification has been provided for any non-convergent algorithms. In this regard, we have paid particular attention to implementation and study of convergent list-mode reconstruction algorithms.

In [9], [10], Hsiao *et al.* have derived a new convergent complete-data ordered subsets EM (C-OSEM) algorithm for histogram-mode reconstruction. They have shown that the proposed algorithm monotonically decreases the complete data objective function, and furthermore converges to the maximum of the log-likelihood function[1]. This algorithm, compared to previous convergent algorithms, has the advantage that it is *accelerated* at the same time as it is convergent (unlike ordinary non-subsetized EM), and does not involve a relaxation schedule (unlike, for instance, RAMLA [11]).

[1]The latter convergence is not guaranteed to be *monotonic*, however, though the authors have always seen this to be the case.

The aforementioned approach can be extended to list-mode reconstruction: starting from first principles [12] or by direct transformation of the histogram-mode algorithm [7], one arrives at the following list-mode reconstruction update equations:

$$\tilde{\lambda}_j^{m,l} = \frac{\lambda_j^{m,l-1}}{\sum_{i=1}^{I} w_i g_{ij}} \sum_{k \in S_l} g_{i_k j} \frac{1}{\sum_{b=1}^{J} g_{i_k b} \lambda_b^{m,l-1}} \tag{2}$$

$$\lambda_j^{m,l} = \sum_{s=1}^{l} \tilde{\lambda}_j^{m,s} + \sum_{s=l+1}^{L} \tilde{\lambda}_j^{m-1,s} \tag{3}$$

where $\tilde{\lambda}_j^{m,l}$ is an *intermediate* image vector produced by the first update Eq. (2), subsequently used by Eq. (3) to arrive at the overall image estimate $\lambda_j^{m,l}$. The algorithm thus takes the form of additive updates in image-space, in that upon arriving at any subset, the intermediate image updates for previous subsets are added to the update for the current subset. We refer to this as the convergent subsetized list-mode EM (CS-LMEM) algorithm.

It must however be noted that the additive nature of the algorithm makes its initial convergence rate relatively slow compared to the ordinary subsetized technique, since the current image estimate is added to the previous image estimates, yielding slow initial improvements in image quality [7]. Subsequently, we have used a hybrid ordinary-convergent subsetized (HOCS) LMEM technique, which uses S-LMEM for a portion of the first iteration, and subsequently switches to the convergent CS-LMEM algorithm.

III. Quantitative Dynamic Image Reconstruction

Our quantitative dynamic image reconstruction scheme consists of dividing the list-mode acquired data set into specified dynamic frames, with the activities within each separately reconstructed. It must be noted here that the activity distribution (within the duration of each frame) is likely not to remain entirely static, and thus use of sequential time subsets is not desirable. In other words, one wishes to minimize the separation in-between the MLEs ($\widehat{\lambda}_{S_l}$) for each of the subsets by minimizing inconsistencies between the activity distributions for the subset. We have thus used an alternative scheme for the definition of the subsets (refer to Fig. 3).

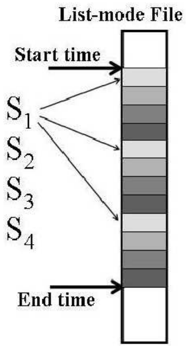

Fig. 3. The frames are divided into, say, three segments, and each segment is in part divided into L portions (L being the number of data subsets).

The extension from 3D imaging to dynamic (or 4D) imaging necessarily requires corrections for the following factors:

i) Detector deadtime The deadtime correction scheme involves a global scaling of the reconstructed images within each frame as determined by the average singles rates within each frame. This is because the singles rates in the HRRT are not noticeably affected by deadtime effects (unlike the coincidence events). Therefore, the major bottleneck in the processing can be attributed to the coincidence detection system which *globally* saturates the acquired coincidences. The scheme involves application of a multiplicative factor, which depends exponentially on the average singles rates, to the reconstructed images.

ii) Decay of radioactivity: Decay correction is relatively the most trivial of all corrections to be applied to reconstructed images. It requires a global scaling of the final reconstructed image by a factor determined by the start and end times within which the events are acquired[2].

In this work, we implemented the HOCS-LMEM algorithm for the HRRT, along with the inclusion of deadtime and decay corrections, applied on the dynamic frames as obtained from the list-mode acquired data. Sixteen subsets were employed: the first 8 subsets in the first iteration were performed using S-LMEM, subsequently switching to CS-LMEM. The detected random events were estimated using delayed-window coincidence detection, and were applied using the delayed coincidence list-mode subtraction technique [7]. The algorithm was tested with a data set spanning a wide range of acquired counts. Images were compared to those obtained using the (i) FORE+2D-FBP, and (ii) 3D-OSEM (with a sinogram bin non-negativity constraint). The former is an analytic technique, making use of the entire 3D data set, and often used as a golden standard for quantitative accuracy (linear property), and the latter is the most commonly employed statistical histogram-mode reconstruction algorithm.

[2]For a given dynamic frame, in ordinary S-LMEM reconstruction, all-but-the-last subsets in the frame merely contribute to improved image estimates, and it is only the counts in the very last subset which determine (quantitatively) the final image. This implies that we need only implement deadtime and decay corrections for the counts occurring within the durations spanned by the very last subset. In convergent CS-LMEM reconstruction, however, images reconstructed from each subset contribute (additively) to the final image, and therefore correction factors need to be applied to all the intermediate images.

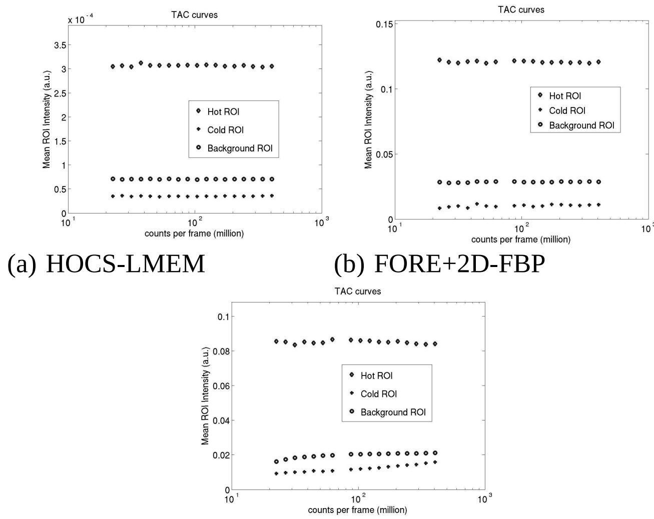

(a) HOCS-LMEM (b) FORE+2D-FBP

(c) OSEM

Fig. 4. Time activity curves (TACs) for 18 frames each 300 s in duration. First frame has a random fraction of 25%, last frame 5%. One iteration and 16 subsets are used in list-mode and OSEM reconstructions.

IV. Methods

Tomograph: Data were acquired on the second generation of the high resolution research tomographs (HRRT) [2]. This HRRT scanner has an octagonal design, with the detector heads consisting of a double 10 mm layer of LSO/LYSO for a total of 119,808 detector crystals.

Phantom study: A 20 cm long, 10 cm radius phantom was used. The phantom had two 5 cm diameter cylindrical inserts, one was filled with water ('cold' insert) and one with a ^{18}F radioactivity concentration of 1.61 μCi/ml ('hot' insert). The phantom itself was filled with a ^{18}F concentration of 0.311 μCi/ml ('background'), yielding a hot insert to background ratio of 5.18. Eighteen dynamic frames (5 minutes each) were considered. The measurement thus covered 4.4 radioisotope half-lives. The random fraction was 25% in the first frame and 5% in the last frame.

Comparison Schemes: We have studies the quantitative accuracy of our dynamic list-mode image reconstruction technique, along with readily available reconstruction software for the HRRT: namely (i) FORE+2D-FBP, and (ii) 3D-OSEM. The following comparisons were performed:

i) Time activity curve (TAC) comparisons: Plots of mean reconstructed voxel intensity (hot, cold and background regions) were obtained for all the reconstructed frames. For a quantitatively accurate reconstruction algorithm, the TAC curves are expected to be constant.

ii) Axial profile comparisons: Mean reconstructed voxel intensities within each axial plane (hot, cold and background regions) were plotted as a function of the axial plane. The corresponding curves for the various frames were overlayed for a visual comparison.

iii) Contrast recovery comparisons: The percent contrasts

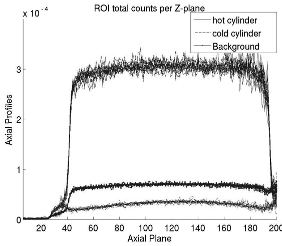

(a) HOCS-LMEM

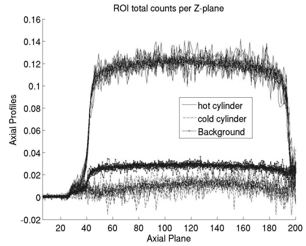

(b) FORE+2D-FBP

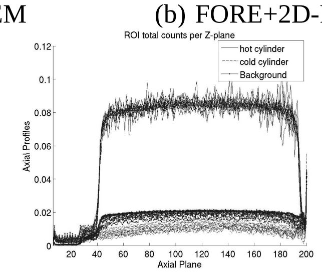

(c) OSEM

Fig. 5. Axial profiles in the hot (top), cold (bottom) and background (middle) regions of the reconstructed images.

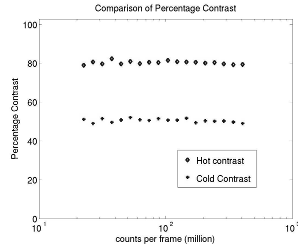

(a) HOCS-LMEM

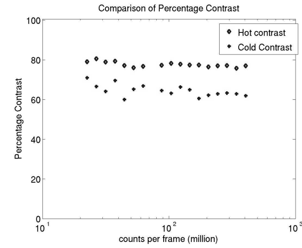

(b) FORE+2D-FBP

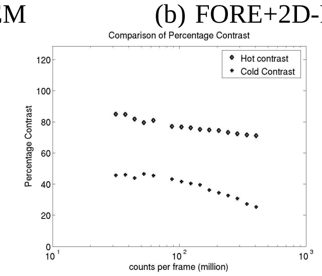

(c) OSEM

Fig. 6. Plots of percentage contrast for the various dynamic frames.

for the hot and cold cylinders were calculated according to the NEMA NU 2001 protocol. The values were depicted as a function of the number of acquired counts per frame.

V. Results and Conclusion

Fig. (4) shows images of time activity curves obtained for the three reconstruction schemes: (a) HOCS-LMEM (b) FORE+2D-FBP and (c) 3D-OSEM. The list-mode algorithm is seen to yield a relatively flat TAC, similar to the FORE+2D-FBP case. However, the histogram-mode scheme yields time activity curves which (especially for the cold and background regions) increase with higher count-rate frames. This is because the current implementation of 3D-OSEM imposes a sinogram non-negativity constraint, which results in a positive bias with frames with higher random fractions (i.e. higher activities).

Axial profiles of the mean ROI activity have been depicted in Fig. (5) for the hot (top), cold (bottom) and background (middle) regions. The profiles for the 18 frames have been drawn overlaying one another. The HOCS-LMEM algorithm is clearly seen to outperform the FORE+2D-FBP algorithm in terms of noise (especially in the background and cold regions). Furthermore, due to the aforementioned zero-thresholding bias, the OSEM algorithm (with a sinogram non-negativity constraint) does not yield overlapping axial profiles for the various frames, and performs poorly. Calculated percentage contrasts are depicted in Fig. (6) for the various frames. Best uniformity is observed for the list-mode technique, while the OSEM approach performs poorly again.

We have thus demonstrated that the statistical list-mode HOCS-LMEM reconstruction algorithm performs very well in terms of quantitative accuracy. This, as well as the efficiency and accuracy benefits of the list-mode approach, render the technique very suitable for dynamic (4D) imaging using the high resolution HRRT scanner. We have also verified that, as predicted, the commonly-imposed sinogram non-negativity constraint (in histogram-mode) reconstruction introduces an *overestimation* bias in the reconstructed images, especially for low-statistic scans with high random fractions.

References

[1] A. J. Reader *et al.*, "Fast accurate iterative reconstruction for low-statistics positron volume imaging", *Phys. Med. Biol.*, vol. 43, pp. 835-846, 1998.

[2] K. Wienhard *et al.*, "The ECAT HRRT: Performance and First Clinical Application of the New High Resolution Research Tomograph", *IEEE Trans. Nucl. Sci.* vol. 49, pp. 104-110, 2002.

[3] W. W. Moses, "Time of Flight in PET Revisited", *IEEE Trans. Nucl. Sci.*, vol. 50, pp. 1325-1330, 2003.

[4] J. A. Kimdon, J. Qi, and W. W. Moses, "Effect of Random and Scatter Fractions in Variance Reduction using Time-of-Flight Information", *IEEE NSS & MIC 2003 conf. rec.*, Portland, OR, Oct 2003.

[5] A. Rahmim *et al.*, "Motion compensation in histogram-mode and list-mode EM reconstructions: beyond the event-driven approach", *IEEE Trans. Nucl. Sci.*, vol. 51, pp. pp. 2588-2596 (2004).

[6] H. M. Hudson and R. S. Larkin, "Accelerated image reconstruction using ordered subsets of projection data", *IEEE Trans. Med. Imag.*, vol. 13, no. 4, pp. 601-609, 1994.

[7] A. Rahmim *et al.*, "Statistical list-mode image reconstruction for the high resolution research tomograph", *Phys. Med. Biol.*, vol. 49, pp. 4239-4258, 2004.

[8] J. Qi and R. H. Huesman, "Theoretical study of lesion detectability of MAP reconstruction using computer observers", *IEEE Trans. Med. Imag.*, vol. 20, pp. 815-822, 2001.

[9] I. T. Hsiao, A. Rangarajan, and G. Gindi, "A provably convergent OS-EM like reconstruction algorithm for emission tomography", *Conf. Rec. SPIE Med. Imaging*, vol. 4684, pp. 10-19, 2002.

[10] I. T. Hsiao, A. Rangarajan, and G. Gindi, "A new convergent MAP reconstruction algorithm for emission tomography using ordered subsets and separable surrogates", *Conf. Rec. IEEE Int. Symp. Biomed. Imaging*, pp. 409-412, 2002.

[11] J. Browne and A. De Pierro, "A row-action alternative to the EM algorithm for maximizing likelihoods in emission tomography", *IEEE Trans. Med. Imag.*, vol. 15, no. 5, pp. 687-699, 1996

[12] P. K. Khurd and G. R. Gindi, "A Globally Convergent Ordered-Subset Algorithm for List-Mode Reconstruction", *IEEE NSS & MIC 2003 conf. rec.*, Portland, OR, Oct 2003.